Bright traveling breathers in media with long-range nonconvex dispersion

Sathyanarayanan Chandramouli, Yifeng Mao, A. Hoefer, and Mark A. Hoefer, and Mark A. Hoefer, and Statistics, University of Massachusetts, Amherst, Amherst, Massachusetts 01003, USA

Department of Applied Mathematics, University of Colorado Boulder, Boulder, Colorado 80309, USA

(Received 17 September 2023; accepted 23 February 2024; published 27 March 2024)

The existence and properties of envelope solitary waves on a periodic traveling-wave background, called traveling breathers, are investigated numerically in representative nonlocal dispersive media. Using a fixed-point computational scheme, a space-time boundary-value problem for bright traveling breather solutions is solved for the weakly nonlinear Benjamin-Bona-Mahony equation, a nonlocal, regularized shallow water wave model, and the strongly nonlinear conduit equation, a nonlocal model of viscous core-annular flows. Curves of unit-mean traveling breather solutions within a three-dimensional parameter space are obtained. Resonance due to nonconvex, rational linear dispersion leads to a nonzero oscillatory background upon which traveling breathers propagate. These solutions exhibit a topological phase jump and so act as defects within the periodic background. For small amplitudes, traveling breathers are well approximated by bright soliton solutions of the nonlinear Schrödinger equation with a negligibly small periodic background. These solutions are numerically continued into the large-amplitude regime as elevation defects on cnoidal or cnoidal-like periodic traveling-wave backgrounds. This study of bright traveling breathers provides insight into systems with nonconvex, nonlocal dispersion that occur in a variety of media such as internal oceanic waves subject to rotation and short, intense optical pulses.

DOI: 10.1103/PhysRevE.109.034212

I. INTRODUCTION

Coherently propagating disturbances such as solitary waves and envelope solitary waves, ubiquitous in nonlinear dispersive media, are formed due to a balance between nonlinearity and dispersion. Envelope solitary waves are generically described by solutions of the cubic nonlinear Schrödinger (NLS) equation subject to two disparate spatial scales: the fast spatial scale corresponding to the wavelength of periodic carrier wave oscillations and the slow-amplitudephase-modulation scale. For an attractive focusing nonlinear medium, the NLS equation admits bright soliton solutions corresponding to a localized sech envelope modulation of a rapidly varying carrier wave. When the carrier phase speed and envelope group speed differ, NLS bright solitons approximate unsteady nonlinear wave packets. Such nonlinear wave packets are also referred to as breathers due to the pulsation or breathing of their internal oscillations. However, the mere existence of approximate NLS bright soliton solutions does not guarantee the existence of breather solutions to a nonlinear dispersive evolution equation.

The canonical evolution equations admitting breather solutions are the sine-Gordon (SG) [1] and modified Korteweg–de Vries (mKdV) [2] equations. These equations are completely integrable by the inverse scattering transform where soliton and breather solutions correspond to discrete eigenvalues of a

corresponding linear spectral problem [1]. A breather solution of SG or mKdV equations corresponds to a pair or quartet of eigenvalues, respectively, which can be interpreted as a bound state of two solitons that decay to zero [2]. Breather solutions to the focusing NLS equation have also been identified as important for modeling rogue wave phenomena [3] and exhibit a nonzero plane-wave background.

The concept of breathers as interacting soliton pairs has been generalized to solutions in which a soliton interacts with a periodic traveling wave, e.g., a cnoidal wave, using a variety of exact solution methods that are available for integrable systems [4–11]. Such solutions have been interpreted as dislocations of a cnoidal background [4]. We refer to these solutions as traveling breathers, which is consistent with their interpretation in lattice systems [12,13]. Traveling breathers are spatially localized on a periodic traveling-wave background and they exhibit two distinct velocities, the phase velocity of the cnoidal background and the envelope velocity of the traveling breather. Other terminology that has been used to describe these coherent structures includes quasibreather [1], localized oscillatory state [14], and nonlocal solitary wave [15].

In the context of interfacial waves that arise in a viscous core-annular flow, coherent bright breather trains were observed to form in computational runs of perturbed, modulationally unstable periodic waves [16]. The nonlinear Schrödinger equation was utilized as an approximate framework to study these wave packets in the weakly nonlinear regime. A follow-up work, involving extensive experiments, generated bright and dark traveling breathers at the interface of such viscous core-annular flows by interacting solitons and

 $[^]st$ sathyanaraya@umass.edu

[†]yifeng.mao@colorado.edu

[‡]hoefer@colorado.edu

cnoidal-like waves [17]. These traveling breathers were seen to robustly persist within the experimental test section for 15–25 oscillatory periods and long distances.

Such breathers and traveling breathers are also prevalent, for example, in fluid dynamics [16,18-21], nonlinear and matter-wave optics [22–29], and magnetic materials [30–32]. However, due to their inherently unsteady character, breather and traveling breather solutions are challenging to obtain. As noted earlier, the exact breather waveforms for integrable systems are constructed through a nonlinear superposition principle based on an application of the Darboux transformation. On the other hand, a common approach to circumvent the reduced analytical tractability associated with nonintegrable systems involves long-time numerical evolution of suitably chosen initial conditions that appear to lead to breather solutions [16,18–21,33,34]. However, due to the existence of small-amplitude radiation accompanying the time evolution, it is difficult to discern whether breather solutions actually exist and, if so, what their properties are. The existence of radiation in these and other computational studies [14,35,36] suggests that a more likely scenario for nonintegrable systems is that breathers are accompanied by an oscillatory background [15,37,38], recent numerical evidence of localized breathers in a nonintegrable equation notwithstanding [39]. In other words, just as solitary-wave solutions in nonintegrable equations generalize the soliton solutions of integrable equations, traveling breather solutions of nonintegrable equations are the natural generalization of breather solutions of integrable equations.

In the present study, we numerically investigate the existence of bright (elevation) traveling breathers to the Benjamin-Bona-Mahony (BBM) and conduit equations, both nonintegrable, nonevolutionary equations [40], by solving a space-time boundary-value problem (BVP) in the comoving reference frame where the envelope speed is zero. The boundary conditions are periodicity in time and space. Multiple one-dimensional families of traveling breather solutions are obtained by numerically continuing the BVP solutions from the weakly nonlinear Schrödinger bright soliton approximation with a given carrier wave number and amplitude. The unit-mean carrier frequency, phase shift, and amplitude are implicitly determined by fixing the breather velocity, the carrier frequency in the comoving frame, and the spatial domain size. Solution branches are obtained by performing continuation in the traveling breather velocity, which is negative for all solution branches computed.

Solutions along a given continuation branch are found to strongly depend upon the initial carrier wave number. When the wave number is sufficiently far from the inflection point of the linear dispersion relation, the carrier background amplitude grows with decreasing velocity while the traveling breather width narrows relative to the carrier wavelength. For initial carrier wave numbers close to the inflection point, the traveling breather envelope width remains large relative to the carrier wavelength. The traveling breather solutions obtained here are found to be dynamically stable under long-time numerical evolution subject to small-amplitude initial noise. Since nonlinear short-pulse optics [22,41] and internal oceanic waves influenced by the earth's rotation [20,33] exhibit similar nonconvex rational dispersion, the traveling

breathers obtained in our study may have implications for these and other applications.

We adapt the Newton-conjugate gradient (NCG) method [42,43] to compute traveling breather solutions. Our parametric continuation scheme is detailed in Sec. IIIB. It is essential to seed the iterative continuation scheme with good initial guesses. We initialize the NCG iterations with weakly nonlinear NLS approximations described in Sec. III.

II. MODEL EQUATION PROPERTIES

The BBM equation in normalized form [44,45]

$$u_t + uu_x - u_{xxt} = 0 ag{1}$$

is a long-wavelength model of weakly nonlinear waves. Equation (1) is not integrable, possessing exactly two other linearly independent conservation laws [46]. Besides the usual space and time translational-invariance properties, the BBM possesses the scaling symmetry

$$u \to u_0 u, \quad x \to x, \quad t \to u_0 t,$$
 (2)

where u_0 is a nonzero real constant. The BBM equation's linear dispersion relation for trigonometric traveling waves on the constant background u_0 is bounded

$$\omega_0(k, u_0) = \frac{u_0 k}{1 + k^2} \tag{3}$$

and exhibits zero dispersion when $u_0 = 0$ or $k = \sqrt{3}$ since

$$\partial_{kk}\omega_0(k, u_0) = \frac{2u_0k(k^2 - 3)}{(k^2 + 1)^3}.$$
 (4)

The bounded nonconvex dispersion (3) distinguishes the short-wave behavior of BBM solutions from those of the Korteweg–de Vries (KdV) equation $u_t + uu_x + u_{xxx} = 0$ with unbounded dispersion and no inflection points for nonzero k.

The BBM equation (1) admits a three-parameter family of periodic traveling-wave solutions in the form of cnoidal waves

$$u(x,t) = \tilde{\beta} + (\tilde{\gamma} - \tilde{\beta})\operatorname{cn}^{2}(z,m),$$

$$z = \left(\frac{\tilde{\gamma} - \tilde{\alpha}}{12\tilde{s}}\right)^{1/2} (x - \tilde{s}t), \quad m = \frac{\tilde{\gamma} - \tilde{\beta}}{\tilde{\gamma} - \tilde{\alpha}}, \quad (5)$$

where $\tilde{\alpha} < \tilde{\beta} < \tilde{\gamma}$, $\tilde{s} = \frac{1}{3}(\tilde{\alpha} + \tilde{\beta} + \tilde{\gamma})$ is the phase velocity, and $\operatorname{cn}(z, m)$ is the Jacobi elliptic cosine function. The cnoidal wave's amplitude a and wave number k are

$$a = \tilde{\gamma} - \tilde{\beta}, \quad k = \frac{2\pi}{L}, \quad L = 4K(m)\sqrt{\frac{3\tilde{s}}{\tilde{\gamma} - \tilde{\alpha}}},$$
 (6)

while its mean is

$$\overline{u} = \tilde{\alpha} + (\tilde{\gamma} - \tilde{\alpha}) \frac{E(m)}{K(m)},\tag{7}$$

where K(m) and E(m) are the complete elliptic integrals of the first and second kinds, respectively. The cnoidal wave (5) limits to a solitary wave when $\tilde{\beta} \to \tilde{\alpha}$ and a constant when $\tilde{\beta} \to \tilde{\gamma}$.

By use of the scaling symmetry (2), we impose the unitmean constraint $\bar{u} = 1$ on the cnoidal wave solutions without loss of generality and therefore constrain $\tilde{\alpha}$, $\tilde{\beta}$, and $\tilde{\gamma}$ via $\overline{u}=1$ in Eq. (7). We parametrize the set of unit-mean periodic traveling-wave solutions to the BBM equation in terms of two parameters such as (a, k). Then its frequency is determined to be $\omega=k\tilde{s}$.

A strongly nonlinear generalization of the BBM equation is the conduit equation [47]

$$A_t + 2AA_z - AA_{tzz} + A_t A_{zz} = 0, (8)$$

modeling large-amplitude long waves along the circular free interface between two viscous fluids with high-viscosity contrast and small Reynolds number [48]. Its linear dispersion relation on the constant background $A_0 > 0$ is similar to the BBM equation (3),

$$\omega_0(k; A_0) = \frac{2A_0k}{1 + A_0k^2}. (9)$$

It is bounded and has an inflection point when $k = \sqrt{3/A_0}$. We mention that, like the BBM equation, the conduit equation is not integrable and possesses at least two independent conservation laws [49]. Finally, the equation satisfies the scaling symmetry

$$A \to A_0 A, \quad z \to A_0^{-1/2} z, \quad t \to A_0^{1/2} t.$$
 (10)

The conduit equation (8) also admits a three-parameter family of periodic traveling-wave solutions [16,50] but an analytical expression for it is not known. Utilizing the scaling symmetry (10), we impose the unit-mean constraint so that the cnoidal-like periodic traveling-wave solutions are parametrized by, e.g., their wave number k and amplitude a.

III. COMPUTATIONAL METHODOLOGY

We begin by introducing the common approach to computing approximate bright breather solutions by assuming weak nonlinearity and scale separation. The NLS equation models the slowly varying envelope $B(\zeta, \tilde{\tau})$ of nearly monochromatic nonlinear wave packets [51,52]. In this regard, the focusing NLS reduction obtained by employing a standard multiple-scale calculation and rescaling takes the form

$$iB_{\tilde{\tau}} + \frac{1}{2}B_{\zeta\zeta} + |B|^2 B = 0.$$
 (11)

The coordinate system associated with Eq. (11) is

$$\zeta = \frac{\epsilon}{\sqrt{\partial_{\tilde{k}\tilde{k}}\omega_0}}(x - \partial_{\tilde{k}}\omega_0 t), \quad \tilde{\tau} = \epsilon^2 t, \tag{12}$$

where $\partial_{\bar{k}}\omega_0$ is the group velocity, $\partial_{\bar{k}\bar{k}}\omega_0$ represents the dispersion curvature, and ϵ is an amplitude scale. The benefit of the NLS approximation is that a simple ordinary differential equation (ODE) can be sought for describing the spatial variation of the envelope $b(\zeta)$, where $B=b(\zeta)\exp(i\mu\tilde{\tau})$ and μ is an amplitude-dependent frequency shift. The well-known sech solution of this ODE, $b\equiv \mathrm{sech}(\zeta)$ and $\mu=\frac{1}{2}$, will be used to seed the continuation algorithm that we describe shortly.

In contrast, the direct computation of traveling breathers requires solving a partial differential equation. We now describe the strategy we adopt to compute BBM and conduit bright traveling breathers as solutions to a space-time boundary-value problem.

A. Space-time boundary-value problem

The BBM and conduit equations are examples of nonevolutionary equations in the form

$$u_t = \mathbb{L}[u, u_t] + \mathbb{N}[u, u_t], \tag{13}$$

where \mathbb{L} is a linear, constant coefficient skew-adjoint differential operator while $\mathbb{N}[u, u_t]$ is in general a nonlinear operator acting on u and u_t . Entering the comoving frame with velocity c ($\chi = x - ct$, $\tau = t$), we recast Eq. (13) as

$$\beta_{\tau} - c\beta_{\chi} - \tilde{\mathbb{L}}[1 + \beta, \beta_{\tau} - c\beta_{\chi}] - \tilde{\mathbb{N}}[1 + \beta, \beta_{\tau} - c\beta_{\chi}] = 0,$$
(14)

where $u(x, t) \equiv 1 + \beta(\chi, \tau)$ and the linear operator $\tilde{\mathbb{L}}$ inherits the skew symmetry. Using the scaling symmetry (2) or (10), we set the background mean to unity, without loss of generality. In this reference frame, the solution is assumed to be time periodic with period T and to rapidly decay to a periodic background in space. Then β has zero mean in the far field in χ due to the unit-mean normalization of u. We truncate the domain $(\chi, \tau) \in [-L, L] \times [0, T]$ and take a finite Fourier product basis for the solution field

$$\beta(\chi, \tau; c, T) \approx \sum_{m=-N}^{N} \alpha_m(\chi) e^{im(2\pi\tau/T)},$$

$$\alpha_m(\chi) \approx \sum_{s=-M}^{M} \hat{\alpha}_{ms} e^{is(2\pi\chi/L)}.$$
(15)

The spatial domain is chosen to be sufficiently large so that boundary effects are negligible, leading to a fully periodic product basis. The actions of the two-dimensional forward and inverse discrete Fourier transforms are denoted by $\mathcal{F}_{2D}(\cdot)$ and $\mathcal{F}_{2D}^{-1}(\cdot)$, respectively.

We now describe the iterative procedure to recover numerical solutions from their weakly nonlinear approximations governed by the NLS equation, which in the co-traveling frame and in terms of fast space and time variables is

$$\beta(\chi, \tau) \approx \frac{\tilde{a}}{2} \operatorname{sech}\left(\frac{\epsilon}{\sqrt{\partial_{\tilde{k}\tilde{k}}\omega_{0}}}\chi\right)$$

$$\times \cos\left[\tilde{k}\chi - \left(\omega_{0} - \frac{\epsilon^{2}}{2} - \tilde{k}\partial_{\tilde{k}}\omega_{0}\right)\tau\right], \quad (16)$$

where $\epsilon = \frac{\tilde{a}\sqrt{\gamma}}{4}$ while the parameters $\gamma(\tilde{k})$ and ω_0 depend on the particular dispersive evolution equation at hand. Having fixed the time period T to the NLS prediction, the solution field β and the envelope velocity c need to be determined. As we will show, the family of unit-mean solutions is three dimensional. While the ansatz (15) for β can be used in Eq. (14), to determine the velocity c, we require an additional condition. Multiplying Eq. (14) by β_{τ} and isolating the terms containing the velocity c results in $\mathcal{H}(\beta) = c\mathcal{G}(\beta)$. Integrating this expression over the entire spatiotemporal domain, we obtain the self-consistent integral condition for c,

$$c = \frac{\int_0^T \int_{-L}^L \mathcal{H}(\beta) d\chi d\tau}{\int_0^T \int_{-L}^L \mathcal{G}(\beta) d\chi d\tau},$$
(17)

provided the denominator is nonzero. Other integral relations for c may similarly be derived. Equation (17) is used because it is found to be robust in the sense that iterations converge, it is efficient in the associated iterative procedure, and we never observe the denominator to go to zero.

We implement the Newton-conjugate gradient algorithm on Eq. (14) subject to the ansatz (15). To recover c and β simultaneously, we update the velocity iteratively at every outer Newton iteration using (17) (see [43] for a similar treatment). Upon insertion of (15) into (14), Newton operator iterations are then applied to Eq. (14). The linearization is symmetrized and inner preconditioned-conjugate gradient iterations are used to solve this positive-semidefinite self-adjoint system, which is expected to converge [42]. The complete velocity-solution profile update algorithm is summarized as

$$\mathbf{P}_{1n}^{\dagger} \mathbf{P}_{1n} \Delta \beta = -\mathbf{P}_{1n}^{\dagger} \mathbf{P}_{0} \beta_{n}, \quad n = 1, 2, \dots$$

$$c_{n} = \frac{\int_{0}^{T} \int_{-L}^{L} \mathcal{H}_{n}(\beta) d\chi d\tau}{\int_{0}^{T} \int_{-L}^{L} \mathcal{G}_{n}(\beta) d\chi d\tau},$$

$$\Delta \beta = \beta_{n+1} - \beta_{n}, \tag{18}$$

where \mathbf{P}_{1n} is the linearization operator at the *n*th Newton iteration, with its adjoint operator represented by $\mathbf{P}_{1n}^{\dagger}$, and $\mathbf{P}_{0}\beta_{n}$ is the residual of Eq. (14) at the *n*th iteration.

We seed the iterations with a sufficiently close initial guess $(\beta_1 \text{ and } c_1)$. For the BBM and conduit equations, the bright solitary-wave solutions of the corresponding NLS reductions give sufficiently close approximations. Iterations are terminated when the residual $\max_{\chi,\tau} |\mathbf{P}_0\beta|$ is less than 10^{-10} . To reduce the condition number of the linear operator $\mathbf{P}_{1n}^{\dagger}\mathbf{P}_{1n}$, it is necessary to introduce an acceleration operator. We follow the guidelines outlined in [42,43]. For Eq. (14), an appropriate acceleration operator at the *n*th Newton iteration is chosen by examining the constant-coefficient part of the symmetrized operator $\mathbf{P}_{1n}^{\dagger}\mathbf{P}_{1n}$, given by $-(\mathbb{B}_n)^2 = -(\partial_{\tau} - c_n\partial_{\chi} - \tilde{\mathbb{L}})^2$. Notably, this operator is positive semidefinite. An appropriate acceleration operator is thus given by the positive-definite operator $\mathbf{M}_n = r - (\mathbb{B}_n)^2$, where r > 0 is a positive number whose choice is arrived at via numerical experiments.

B. Parametrization and numerical continuation

Having described the computation of a numerically accurate waveform in the weakly nonlinear regime, we now lay out the continuation procedure to obtain a family of solutions from this known solution. Implicit to the product basis representation in Eq. (15) for spatially localized unit-mean breathers, we have a two-parameter characterization (envelope velocity c and time period T). Given a known solution, we perform a line search for a fixed time period T, by varying the velocity c parameter (referred to as c continuation). We perform several such line searches starting from different weakly nonlinear solutions. The search algorithm at the jth c-continuation step is

$$\mathbf{P}_{1n}^{\dagger(j)}\mathbf{P}_{1n}^{(j)}\Delta\beta = -\mathbf{P}_{1n}^{\dagger(j)}\mathbf{P}_{0}^{(j)}\beta_{n}, \quad n = 1, 2, \dots,$$
 (19)

where the iterations are seeded the previous solution $(\beta^{(j-1)})$ and $c^{(j-1)}$), while a traveling breather with fixed velocity $c^{(j)} = c^{(j-1)} + \delta c$ is sought. Note that similar space-time

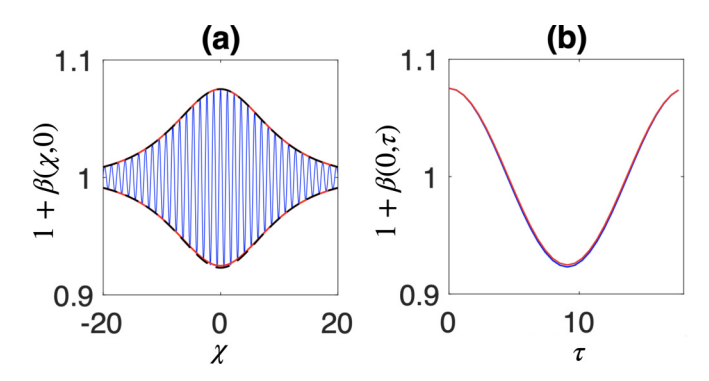


FIG. 1. (a) Traveling breather in the weakly nonlinear regime (blue solid line) of family 1 with $T \approx 18.180$ and $c \approx -0.031$ on a spatial domain with L = 400. The numerical envelope (black dashed line) is compared to the NLS bright soliton envelope (red solid line). (b) Evaluation of the traveling breather at $\chi = 0$ over one period (blue solid line) compared with the leading-order NLS approximation (16) (red solid line).

boundary-value computations have been used to compute breathers and traveling breathers in discrete lattice systems [13] and modified NLS-type models [53,54].

IV. RESULTS

A. BBM bright traveling breather solutions

We compute five branches of BBM traveling breathers, bifurcating from the focusing NLS limit. The edge of the focusing regime [$\sigma > 0$ in Eq. (11)] of the NLS reduction is marked by the inflection point of the unit-mean linear dispersion relation (3) $\tilde{k} = \sqrt{3} \approx 1.73$. It is crucial to initialize the Newton iterations with an accurate initial guess in the nearly monochromatic regime for convergence to traveling breathers. In order to use a NLS bright soliton as the initial seed for the continuation procedure, it is necessary to initialize the carrier wave number $\tilde{k} > \sqrt{3}$. The five traveling breather branches are characterized by the carrier wave numbers

$$\tilde{k}^{(1)} \approx 5.42 > \tilde{k}^{(2,3)} \approx 3.79 > \tilde{k}^{(4)} \approx 3.01 > \tilde{k}^{(5)} \approx 2.42.$$
(20)

We refer to each of these branches as families 1, 2, 3, 4, and 5, respectively. We perform the computations on large domains for each of the breather families 1–5, with $2L \in \{400, 200, 500, 500, 500\}$, respectively. The spatial discretization for all the computed families is $\Delta x = 2L/2M = 0.08$, while N = 16 (32 Fourier modes) is found to be an appropriate discretization in time. The NLS approximations provide good initial guesses for computing traveling breathers with carrier wave numbers $\tilde{k} > 2.4$.

The initial guess for NCG iterations is the bright soliton solution of the NLS equation (11), where $\gamma(\tilde{k})=(5\tilde{k}^2+3)/(6\tilde{k}^3+18\tilde{k})$ and ω_0 [Eq. (3)], $\partial_{\tilde{k}}\omega_0$, and $\partial_{\tilde{k}\tilde{k}}\omega_0$ are evaluated at $\tilde{k}=\tilde{k}^{(j)}$ for some j and $u_0=1$. We initialize the computations with $\tilde{a}\approx 0.15$. The NLS bright soliton envelope is localized, whereas the computed traveling breathers are found to exhibit oscillatory tails, albeit very small for small \tilde{a} . It is convenient to introduce the traveling breather frequency in the comoving frame $\Omega=2\pi/T$. In Fig. 1 we compare

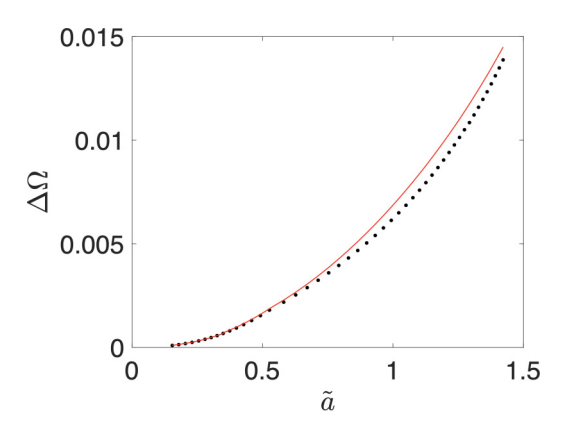


FIG. 2. Traveling breather frequency shift from computation (black dotted line) and predicted (red solid line) traveling breathers.

the computed and NLS bright soliton profiles for the first traveling breather of family 1. The profiles agree to within 1%. The numerical envelope profiles are extracted using the Hilbert transform [21]. Furthermore, the traveling breather frequency Ω and velocity c are within 1% of the bright soliton predictions (16). The first computed solution for all traveling breather families exhibits similar agreement to the NLS bright soliton prediction (16).

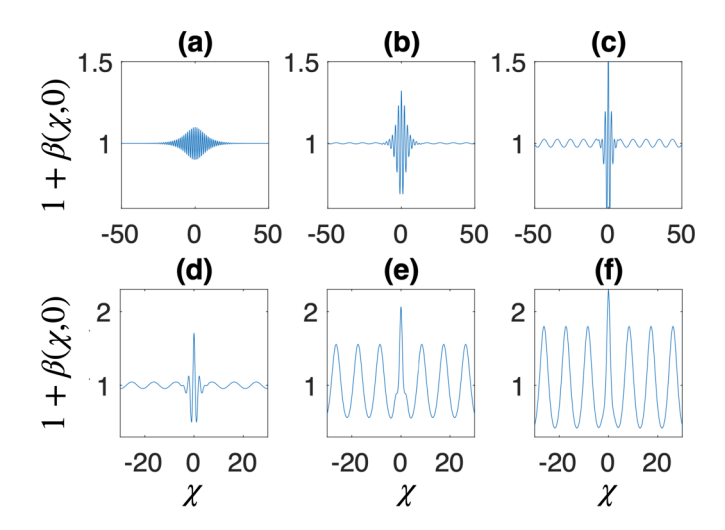
To recover other traveling breathers, we apply c continuation. The continuation procedure is found to introduce a shift in the wave mean. At the end of c continuation for each family, we scale all the obtained traveling breathers to unit mean by utilizing Eq. (2). Consequently, although we fix the time period T during continuation, the rescaling to unit mean implies that the time period of the computed traveling breathers changes across each family.

Performing c continuation, we observe an increase in traveling breather amplitude with decreasing c. Define the traveling breather nonlinear frequency shift

$$\Delta\Omega = \Omega_0 - \Omega,\tag{21}$$

where $\Omega_0 = \omega_0 - \tilde{k} \partial_{\tilde{k}} \omega_0$ is the linear frequency in the comoving frame. In Fig. 2(a) the prediction $\Delta\Omega = \epsilon^2/2$ from Eq. (16) is compared with the computed frequency shift (21) for family 1 across a range of amplitudes. As expected, there is good agreement at low amplitudes and deviation at large amplitudes.

Figure 3 displays six traveling breather solutions from family 1 at $\tau = 0$. To the eye, the solution in Fig. 3(a) appears localized, decaying to 1 as $|\chi| \to \infty$. In fact, all computed traveling breathers exhibit an oscillatory background. This is consistent with rigorous studies of breathers in Klein-Gordon equations where it was proven that, in the nonintegrable case, small-amplitude breather solutions are accompanied by exponentially small oscillatory tails [37,38]. As the traveling breather amplitude increases in Fig. 3, the oscillatory background becomes more prominent, eventually reaching an amplitude that is comparable to the traveling breather itself. The increase in carrier amplitude is accompanied by a narrowing of the traveling breather's width such that, in Figs. 3(e) and 3(f), the traveling breather itself is narrower than the carrier wavelength. We point to some other general trends within the computed solution families. The upper limit to the traveling



traveling FIG. 3. Family 1 of breather solutions $(T, c) \approx 16.917, -0.036,$ BBM equation with (a) $(T, c) \approx 11.969, -0.076,$ (c) $(T, c) \approx 11.942, -0.079,$ (d) $(T, c) \approx 11.906, -0.082$, (e) $(T, c) \approx 11.316, -0.099$, and (f) $(T, c) \approx 10.682, -0.129.$

breather velocity c is approached in the vanishing amplitude regime so that it is the linear group velocity for family $j:c<\partial_{\tilde{k}}\omega_0(\tilde{k}^{(j)},1)$, implying that all traveling breather velocities are negative. On the other hand, the computations do not apparently indicate a lower bound to the breather velocities:

$$c < \partial_{\tilde{k}}\omega_0(\tilde{k}^{(j)}, 1) < 0. \tag{22}$$

This implies that, when bifurcating from the NLS bright soliton, traveling breather velocities are always negative, i.e., $c \in (-\infty, 0)$.

The traveling breather envelope amplitude is defined as

$$\tilde{a} = \max_{\tau \in [0,T]} \beta(0,\tau) - \min_{\tau \in [0,T]} \beta(0,\tau). \tag{23}$$

In Fig. 3, we observe that the traveling breather width narrows relative to the carrier wavelength as \tilde{a} increases.

Let us count the number of parameters characterizing the traveling breather solutions. In addition to the velocity c and time period T, the existence of the periodic background introduces two additional parameters, the carrier amplitude

$$a = \limsup_{\chi \to \infty} \beta(\chi, 0) - \liminf_{\chi \to \infty} \beta(\chi, 0)$$
 (24)

and the carrier wave number k [cf. Eq. (6)], with the carrier frequency $\omega = \omega(k, a)$ uniquely determined by the unit-mean $(\overline{u} = 1)$ constraint (7). Since the traveling breather frequency in the comoving frame is known $\Omega = 2\pi/T$, we have the additional compatibility relation

$$\omega(k,a) - ck = \Omega. \tag{25}$$

Traveling breathers impart a phase shift to the periodic background, which we normalize to $\sigma \in [-\pi, \pi]$. The phase shift quantifies the amount by which the periodic background has advanced or receded across the traveling breather core. In our computations, the phase shift is implicitly determined by the spatial domain [-L, L] and the imposition of spatially periodic boundary conditions. The number of carrier wavelengths that fit in the domain is $N = |Lk/\pi|$, so the difference

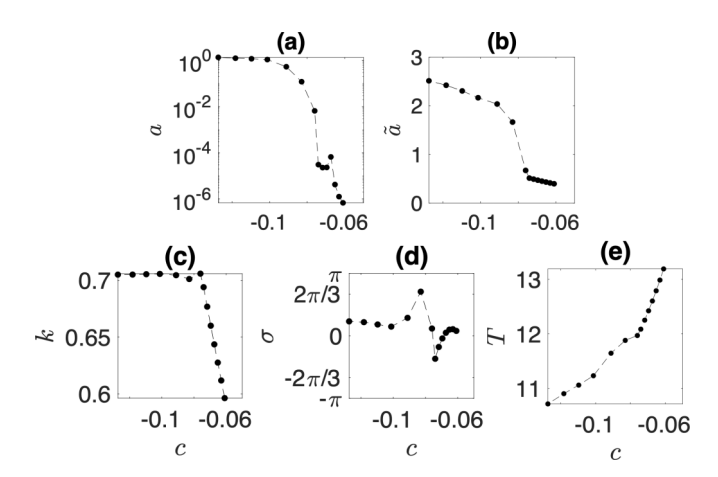


FIG. 4. Variation of the (a) periodic background amplitude (23), (b) breather amplitude (24), (c) periodic background wave number, (d) phase shift σ (26), and (e) time period T with breather velocity c for family 1 of BBM breathers.

 $\Delta \chi = 2L - 2\pi N/k \geqslant 0$ represents the spatial mismatch. The normalized phase shift is determined according to

$$\sigma = \begin{cases} k\Delta\chi, & k\Delta\chi < \pi \\ k\Delta\chi - 2\pi, & k\Delta\chi > \pi. \end{cases}$$
 (26)

For our traveling breather computations, we input the four parameters $c, T, L, \overline{u} = 1$. The two relations (25) and (26) can be used to determine a and σ . Thus, unit-mean traveling breathers constitute a three-parameter family of solutions. In Fig. 4 we show how the parameters a, \tilde{a} , k, σ , and T vary with the breather velocity c for family 1. As c is decreased, the parameters a, \tilde{a} , and k increase, with k and a rapidly approaching an asymptotic value in the strongly nonlinear regime. The phase shift σ also limits to an asymptotic value for large-amplitude (more negative c) traveling breathers, while displaying both positive and negative phase shifts across the range of velocities. By continuity, there is a traveling breather exhibiting a zero phase shift. Finally, we remark that, since we initialized the computations of family 1 with the NLS bright soliton (16) where $\tilde{a} \approx 0.15$, the largest value of c, $c_{\rm max} \approx -0.031$, is less than the theoretical upper bound (22) $\partial_{\tilde{k}}\omega_0(\tilde{k}^{(1)},1)\approx -0.0308$, which applies in the limit $\tilde{a}\to 0$. We did not attempt to compute smaller-amplitude solutions. The smallest velocity for which we compute a traveling breather solution is $c \approx -0.129$, which is shown in Fig. 3(f). At this point, the existence of a lower bound for breather velocities is unknown but remains interesting for future investigations. The fifth branch of computed traveling breathers crossing the linear inflection point shown in Figs. 5(a)-5(c) merits special mention. Given their proximity to the zero-dispersion line ($\Omega_0 = 3\sqrt{3}/8$) in the weakly nonlinear regime, they display a prominent periodic background even for small amplitudes. For amplitudes $0.16 \le \tilde{a} \le 0.62$, the carrier wave number of the breather core is found to lie in the interval $\tilde{k} \in [1.67, 2.42]$, which is below the linear dispersion inflection point $\tilde{k} = \sqrt{3} \approx 1.73$. When $\tilde{k} < \sqrt{3}$, the NLS equation (11) is repulsive or defocusing. This persistence of bright traveling breathers across the zero-dispersion line into

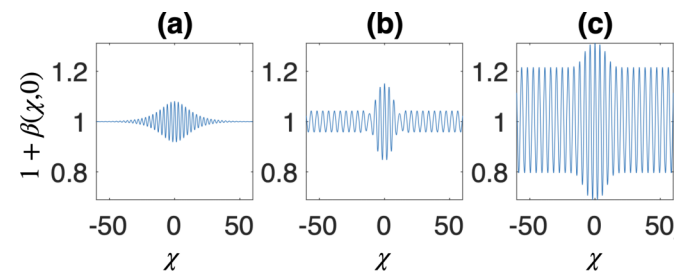


FIG. 5. Family 5 of BBM traveling breathers with (a) $(\tilde{a}, c, T) \approx 0.162, -0.110, 10.142$, (b) $(\tilde{a}, c, T) \approx 0.306, -0.124, 9.708$, and (c) $(\tilde{a}, c, T) \approx 0.623, -0.133, 9.486$.

the defocusing regime is an intriguing feature, suggesting the need for a higher-order NLS model to describe them [24,55].

In order to assess how close to the NLS regime computed traveling breathers are, we plot the relationship between the traveling breather frequency in the comoving frame with frequency Ω and velocity c for each solution family in Fig. 6(a). To compare with the NLS bright soliton (16), we obtain a relationship between the linear frequency in the comoving frame $\Omega_0 = 2\tilde{k}^3/(1+\tilde{k}^2)^2$ and the linear group velocity $c_0 = \partial_{\tilde{k}}\omega_0 = (1-\tilde{k}^2)/(1+\tilde{k}^2)^2$ by eliminating \tilde{k} to obtain

$$\Omega_0(c_0) = 2\sqrt{-2c_0} \frac{[(2c_0+1) + \sqrt{8c_0+1}]^{3/2}}{(1+\sqrt{8c_0+1})^2},$$
 (27)

where $-\frac{1}{8} < c_0 < 0$ in the focusing regime. The computed traveling breathers lie close to the $\Omega_0(c_0)$ curve in Fig. 6(a) for small amplitudes and depart from the curve for larger amplitudes or fewer carrier wave oscillations in the breather core. We conclude this section with a concise representation of all the computed traveling breather families in Fig. 6(b). To this end, a convenient set of defining parameters is the traveling breather amplitude \tilde{a} , the velocity c, and the time period in the comoving frame T (or the associated angular frequency $\Omega = 2\pi/T$). From Eqs. (16) and (21) with $\Delta\Omega = \epsilon^2/2$, the time period T in the NLS approximation is

$$\mathcal{T}(\tilde{a},c) = \frac{2\pi}{\Omega} = \frac{2\pi}{\Omega_0(c) - \frac{\tilde{a}^2}{22}\gamma(c)},\tag{28}$$

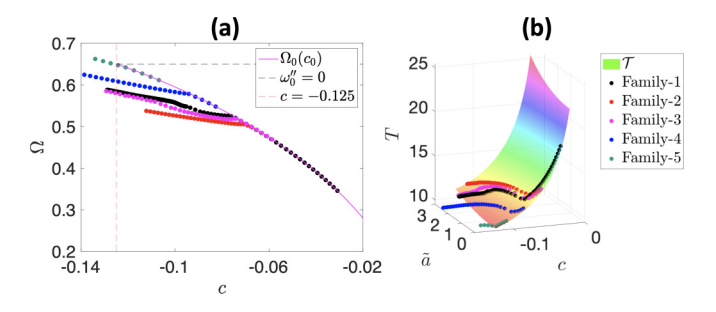


FIG. 6. (a) Projections in amplitude of the velocity (c)-frequency (Ω) relation of the five traveling breather branches. (b) Computed unit-mean traveling breathers from the five families (closed circles) and the weakly nonlinear prediction $T=\mathcal{T}$ (28) (colored surface).

where $\gamma(c) = \frac{\sqrt{-2c}}{6\sqrt{(2c+1)+\sqrt{8c+1}}} \frac{-5-4c-5\sqrt{8c+1}}{4c-1-\sqrt{8c+1}}$ and $\tilde{k}(c) \equiv \sqrt{\frac{-(2c+1)-\sqrt{8c+1}}{2c}}$ is determined by inverting $c = \partial_{\tilde{k}}\omega_0(\tilde{k},1)$. All NLS-like envelope solitons that enclose several carrier wave oscillations within the breather core, lie close to the two-parameter surface $T = \mathcal{T}(\tilde{a}, c)$. These breather cores decay rapidly to a very-small-amplitude ($a \ll 1$) periodic background. This surface is depicted in Fig. 6(b). The parameters \tilde{a} , c, and T associated with each computed traveling breather are also rendered in the figure. In the weakly nonlinear regime, the traveling breathers of all five families reside close to $T = \mathcal{T}(\tilde{a}, c)$. Eventually, they depart from the surface, exhibiting a larger time period than weakly nonlinear theory predicts. For families 1–4, the strongly nonlinear breathers limit to enclosing very few carrier oscillations within the breather cores, with the envelope widths being comparable to the cnoidal (background) carrier wavelength. An exception in this regard is family 5, wherein the breather core possesses a slowly varying envelope despite a large amplitude \tilde{a} . As a final remark, we draw attention to families 2 and 3, computed on domains with L = 100and 250, respectively, and seeded with an identical NLS envelope soliton (see Fig. 6). The role of the computational domain length as an additional parameter (besides c and T) is clear, as the scatter plots diverge noticeably beyond the weakly nonlinear regime owing to the different induced phase shift σ .

B. Conduit equation bright traveling breather solutions

The examination of BBM bright traveling breathers has primed us for an investigation of their analogs in the conduit equation, which has an identical unit-mean linear dispersion relation.

The computations are initialized using the weakly nonlinear NLS approximation (16) with $\tilde{k} = 4$ and $\tilde{a} \approx 0.38$. As before, the amplitude scale in Eq. (16) is defined by $\epsilon =$ $\tilde{a}\gamma/4$, with $\gamma = (8\tilde{k}^4 + 5\tilde{k}^2 + 3)/(3\tilde{k}^5 + 12\tilde{k}^3 + 9\tilde{k})$. While continuing the branch of traveling breathers, we observe the familiar trends associated with a shifting wave mean and the emergence of a periodic carrier background. After this family, referred to as family 1, is computed, we apply the scaling symmetry (10) to normalize all the breathers to unit mean. The continuation runs slow down once the number of cycles of carrier wave oscillations in the breather core limit to three, in contrast to the continuation runs for BBM breathers, where the limit was at one cycle. Like in the case of BBM breathers, the group velocity $\partial_{\tilde{k}}\omega_0 = 2(1-\tilde{k}^2)/(1+\tilde{k}^2)^2$ in the weakly nonlinear regime appears to be an upper limit for conduit breathers. This precludes breathers propagating with positive velocity because $\tilde{k} > \sqrt{3} > 1$. Moreover, a lower limit for breather velocity is not apparent from the computational results. On the other hand, a point of difference with the BBM waveforms is a pronounced asymmetry, which tends to bound the conduit wave profiles away from zero.

To illustrate these trends, we present a few representative conduit breathers from family 1 in Fig. 7. The relevant computations are performed on a spatial domain of length 2L = 120 with spatial step $\Delta x = \frac{2L}{2M} \approx 0.06$ while N = 16 (32 Fourier modes) provides the temporal discretization. The

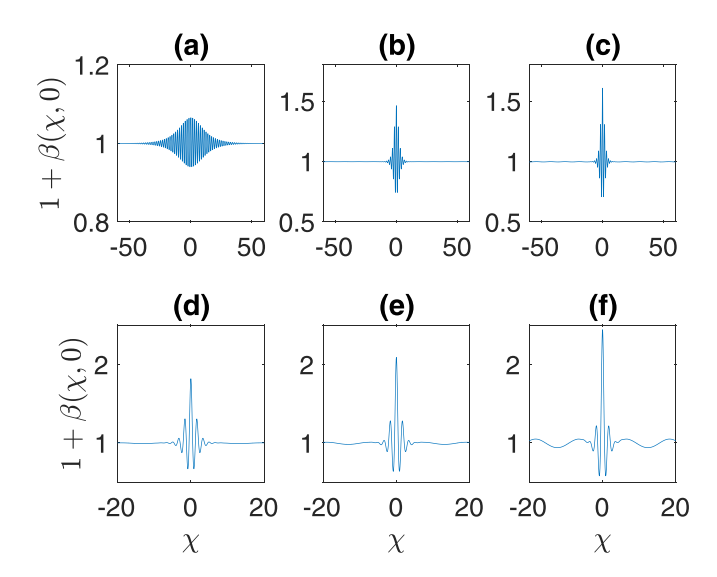


FIG. 7. Family 1 of traveling breathers of the conduit equation with (a) $(T,c) \approx 7.172, -0.101$, (b) $(T,c) \approx 7.093, -0.106$, (c) $(T,c) \approx 7.079, -0.107$, (d) $(T,c) \approx 7.073, -0.109$, (e) $(T,c) \approx 7.072, -0.111$, and (f) $(T,c) \approx 7.116, -0.113$.

entire branch is contained within a relatively small velocity interval of width approximately equal to 0.012.

In Fig. 8 we show how the identifying parameters a, \tilde{a} , k, σ , and T vary with the breather velocity c for family 1, upon the emergence of the periodic background. With an increasing magnitude of the wave-packet velocities, increasing trends in a and \tilde{a} are observed, while k displays slight variation. The phase jump σ is negative for all breathers in this branch. Given the strongly nonlinear nature of the conduit equation, it is interesting to check how close the traveling breathers are to the NLS regime. To this end, as before, the time period T, velocity c, and amplitude \tilde{a} form a set of identifying parameters. Moreover, the time period in the NLS approximation is given in Eq. (28), where, for the conduit equation, the linear frequency $\Omega_0(c)$ is

$$\Omega_0(c) = \frac{2\sqrt{-c}(1+c+\sqrt{4c+1})^{3/2}}{2c+1+\sqrt{4c+1}},$$
 (29)

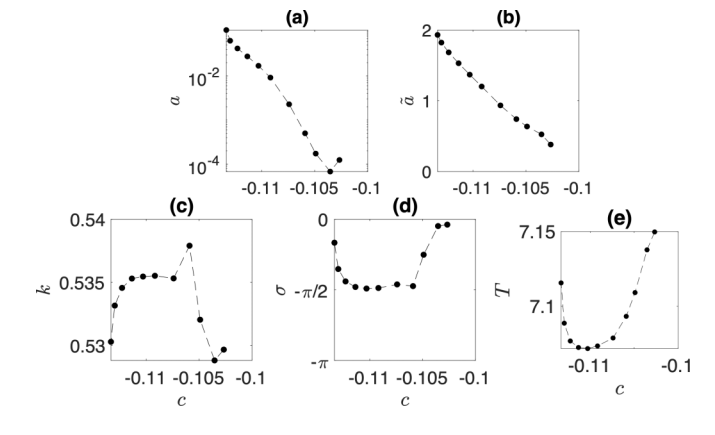


FIG. 8. Variation of the (a) periodic background amplitude (23), (b) breather amplitude (24), (c) periodic background wave number, (d) phase shift σ (26), and (e) time period T with breather velocity c for family 1 of conduit breathers.

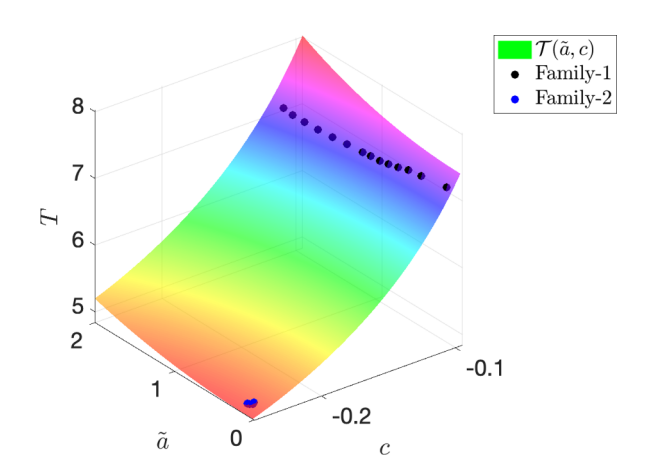


FIG. 9. Computed unit-mean traveling breathers from the families (closed circles) and the weakly nonlinear prediction $T = \mathcal{T}$ (28) (colored surface).

thus necessitating $-\frac{1}{4} < c_0 < 0$ for a real frequency. Additionally, $\gamma(c)$ is defined to be

$$\gamma(c) = \frac{\sqrt{-c}}{3\sqrt{c+1+\sqrt{4c+1}}} \times \frac{16+16\sqrt{4c+1}+43c+11c\sqrt{4c+1}+6c^2}{2+2\sqrt{4c+1}+2c-2c\sqrt{4c+1}}.$$
(30)

The NLS surface for the conduit equation $\mathcal{T}(\tilde{a},c)$ is shown in Fig. 9. For appreciably small intervals in velocity, timeperiod, and breather amplitudes, the wave packets reside on the $\mathcal{T}(\tilde{a},c)$ surface and thereafter lie entirely below it.

We also investigate the existence and form of weakly non-linear conduit breathers near the zero-dispersion line. To this end, we initiate the computations with an appropriate NLS initial guess. We recover a delocalized wave packet with a nearly monochromatic amplitude-modulated core with $\tilde{k}=2$ [see Fig. 10(a)]. We seed the c-continuation algorithm with this wave packet, to obtain the breather in Fig. 10(b). This wave packet is characterized by core carrier wave oscillations with wave number $\tilde{k}=1.8$. The continuation procedure is

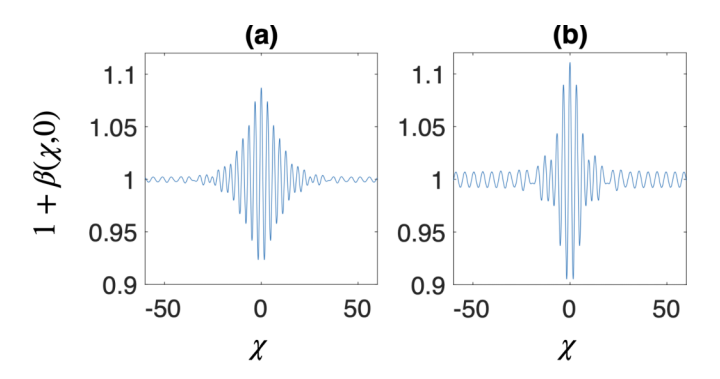


FIG. 10. Family 2 of conduit weakly nonlinear wave packets near the zero-dispersion line, characterized by (a) carrier wave number $\tilde{k} \approx 2$ and $(\tilde{a}, c, T) \approx 0.166, -0.240, 4.907$ and (b) $\tilde{k} \approx 1.8$ and $(\tilde{a}, c, T) \approx 0.210, -0.243, 4.886$.

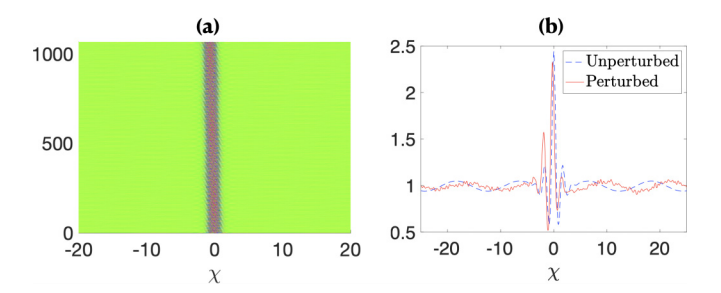


FIG. 11. Evolution of a perturbed strongly nonlinear conduit traveling breather from family 1. (a) Contour plot describing the spatiotemporal structure of the perturbed waveform when evolved to $t = 150T \approx 1067$. (b) Time snapshots of the perturbed (red solid line) and unperturbed waveforms (blue dashed line) at the end time, pointing to the coherence of the breather.

seen to slow down significantly thereafter. It is remarkable that even for such small-amplitude traveling breathers, there is a relatively large-amplitude periodic background, which points to the operable higher-order dispersive effects therein. At this point, the existence of bright wave packets across the zero-dispersion line is unclear but is interesting for future investigation.

The strongly nonlinear nature of the conduit equation, coupled with the large conditioning numbers of the symmetrized system of linear equations at each Newton step, result in reduced computational tractability of the continuation algorithm.

C. Dynamic stability of breathers

We numerically investigate the dynamic stability of computed BBM and conduit traveling breathers with direct numerical simulations. The initial condition consists of a numerically computed traveling breather solution $1 + \beta(\chi, \tau)$ evaluated at $\tau = 0$ that is multiplicatively perturbed: u(x, 0) = $[1 + \beta(x, 0)][1 + \Delta(x)]$ for the BBM equation and similarly for the conduit equation. A smooth perturbation function Δ is constructed from a spatially periodic disturbance with random Fourier series coefficients that is band limited and scaled to have a peak amplitude of 0.05. We employ the standard fourth-order Runge-Kutta explicit time-stepping scheme along with a Fourier discretization in space similar to [16,56]. We perform long-time numerical integration for more than 100 breather periods T of two perturbed traveling breather solutions, one weakly nonlinear and the other strongly nonlinear, in each of the seven computed wave families (five BBM and two conduit families). All exhibit similar dynamical behavior. A representative example of a numerically evolved, perturbed strongly nonlinear breather solution from family 1 of the conduit equation compared with the unperturbed breather is shown in Figs. 11(a) and 11(b). The traveling breather core is slightly delayed after an evolution time of 150T. Despite the 5% initial perturbation and long evolution time, the breather retains its coherence.

V. DISCUSSION

Branches of bright traveling breathers have been computed as solutions to a space-time boundary-value problem

for the BBM and conduit equations. For both we found that traveling breathers are approximated by NLS envelope bright solitons for small amplitudes and carrier wave numbers sufficiently deep in the negative dispersion regime. An emergent feature of traveling breathers in the weakly nonlinear regime was delocalization, signified by the presence of a propagating periodic background. While the NLS approximation remains accurate in the traveling breather core, it is necessary to examine the effects of higher-order dispersive corrections to explain the delocalization, which we briefly describe now.

A convenient framework to understand delocalization is the third-order NLS (TNLS) equation

$$iB_{\tau} + \frac{B_{\zeta\zeta}}{2} + |B|^2 B = i\epsilon' B_{\zeta\zeta\zeta}, \quad 0 < \epsilon' \ll 1,$$
 (31)

where $\epsilon' = \epsilon (\partial_{\bar{k}\bar{k}\bar{k}}\omega_0)/6(\partial_{\bar{k}\bar{k}}\omega_0)^{3/2}$, the slow, traveling spatial coordinate ζ is defined in Eq. (12), and ϵ is the amplitude scale [cf. Eq. (11)]. Without loss of generality, we consider the usual unit amplitude NLS envelope soliton $B(\zeta, \tau) = \text{sech}(\zeta) \exp(i\tau/2)$. Linearizing (31) about the soliton and seeking a resonant solution with the same frequency of the form $\exp[i(\kappa \zeta + \frac{\tau}{2})]$, we obtain the cubic equation for κ ,

$$\epsilon' \kappa^3 + \frac{1}{2} \kappa^2 + \frac{1}{2} = 0,$$
 (32)

which admits exactly one short-wave solution $\kappa_0 \sim -\frac{1}{2\epsilon'}$, $|\kappa_0| \gg 1$ as $\epsilon' \to 0$. This resonance with the linear spectrum has two implications: (a) NLS solitons radiate short waves when subject to weak third-order dispersion and (b) steady solutions to Eq. (31), $B(\zeta,\tau) \equiv A(\zeta - \epsilon' c'\tau) \exp[i(\tau/2)]$, are delocalized. Both the unsteady and steady problems are studied under the framework of exponential asymptotics (see [57]), which yields estimates for the amplitudes of the one-sided short-wave radiation emitted by NLS solitons and the far-field $(\zeta \to \pm \infty)$ tails of the steady delocalized waveforms.

An examination of the steady ODE problem reveals that $A(\xi)$ must be exponentially small in ϵ' as $|\xi| \to \infty$. The complex-valued profile $A(\xi)$ exhibits a nonzero phase jump. The implications of this perturbative analysis for weakly nonlinear traveling breathers are that they generically admit a parametrization in terms of the carrier wave number, traveling breather amplitude, and phase jump, respectively. Moreover, this exponential asymptotic result corroborates our computational finding of small-amplitude traveling breathers with nearly localized spatial waveforms.

The wave number of the resonant wave in the fast spatial coordinate x is $\tilde{k}_1 \equiv \tilde{k} + \kappa_0 \frac{\epsilon}{\sqrt{\partial_{\tilde{k}\tilde{k}}\omega_0}} \sim \tilde{k} - 3(\partial_{\tilde{k}\tilde{k}}\omega_0/\partial_{\tilde{k}\tilde{k}\tilde{k}}\omega_0)$. This TNLS prediction is viable provided $|\partial_{\tilde{k}\tilde{k}}\omega_0/\partial_{\tilde{k}\tilde{k}\tilde{k}}\omega_0| \ll 1$. We have compared this wave-number prediction for the BBM and conduit dispersion with the computed traveling breather solutions and observed a significant discrepancy in the interval $\tilde{k} \in [3, 3.5]$ for nearly monochromatic BBM (or conduit) breathers. The relative errors here were found to be as large as 1600%. On the other hand, in the interval $\tilde{k} \in [1.74, 1.9]$, the relative errors were contained below 20% and were found to be as low as 6% for $\tilde{k} \approx 1.8$. This discrepancy is attributed to the intricate structure of the

dispersion relations (3) and (9) for which $\partial_{\tilde{k}\tilde{k}}\omega_0$ is zero when $\tilde{k}=\sqrt{2}+1$ while $\partial_{\tilde{k}\tilde{k}}\omega_0$ is zero at $\tilde{k}=\sqrt{3}$. We suspect that to complete the characterization of the traveling breather periodic background, a cubic NLS model incorporating the full dispersion of these nonlocal models may be required.

Another implication of the BBM-conduit nonconvex dispersion relation is the persistence of traveling bright breathers in the weakly nonlinear defocusing regime (cf. Fig. 5). A preliminary insight into this persistence can be gained within a TNLS framework [24,55], where it was shown that traveling breathers near the zero-dispersion point manifest a bright or antidark waveform instead.

VI. CONCLUSION

In summary, we have introduced a direct computational method for traveling bright breathers of nonlinear dispersive equations. Multiple families of BBM and conduit equation traveling breathers have been obtained. In the weakly nonlinear regime, these limit to amplitude-modulated wave packets that are well approximated by the NLS equation. In the strongly nonlinear regime, these traveling breathers were seen to be delocalized, bright modulation defects on cnoidaltype carrier waves. Large-amplitude BBM breathers were seen to have more pronounced cnoidal backgrounds than the conduit counterparts we computed. Our computations indicate that BBM and conduit bright traveling breathers bifurcating from NLS bright solitons propagate with negative velocities only and thus it is required to turn to an alternate setup to what is currently being employed, for their experimental generation [17]. Finally, BBM and conduit traveling breather solutions were found to be dynamically stable over the course of long-time numerical evolution of their initially perturbed waveforms. A more detailed study investigating the stability of these traveling breathers using Floquet theory is possible future work. Another interesting problem is the experimental generation of bright breather trains and of even a breather gas, from an unstable periodic wave [16]. The latter could also form the basis for future investigations in other relevant geophysical [20,33] or short-pulse optical scenarios [22,41].

Yet another extension of the present work is the computation of bright and dark traveling breathers [11] which are generated in the KdV equation via the interaction of solitons and cnoidal waves [4]. Such classes of traveling breathers have been observed experimentally over wide amplitude ranges in [17] and have been seen to exhibit qualitatively similar properties to their asymptotic KdV reductions. An open question is how these solutions relate to the bright breathers computed here. Can soliton-cnoidal wave interaction solutions be continued to the bright traveling breather solutions obtained here that bifurcate from bright soliton solutions of the focusing NLS equation? Our computational method could help establish the existence and properties of such dark and bright traveling breathers in the absence of integrable structure. A tantalizing problem is the existence of more general two-phase solutions that could also be explored using a similar computational framework.

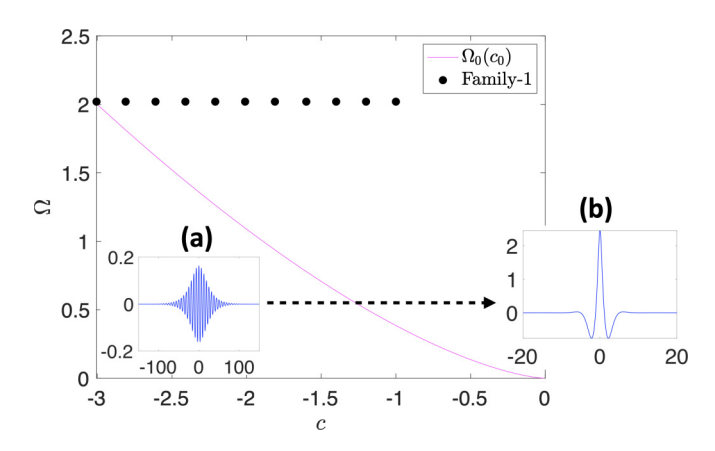


FIG. 12. Continuation path (black dots) marked in the c- Ω phase plane; in the weakly nonlinear regime the path approaches the linear dispersion curve [magenta curve, $\Omega_0(c_0)$] as $c \to -3$. The inset shows slices at $\tau = 0$ of (a) the computed weakly nonlinear mKdV breather and (b) a strongly nonlinear breather.

ACKNOWLEDGMENTS

Our work reached fruition thanks to the inspiring discussions we had with Dr. P. Sprenger and Dr. Z. Musslimani, both of whom we gratefully acknowledge.

APPENDIX: VALIDATION OF THE NCG ALGORITHM ON MKDV BREATHERS

The integrable [58] focusing mKdV equation

$$u_t + 3u^2 u_x + u_{xxx} = 0 (A1)$$

is known to possess bright breathers with closed-form expressions. We assess the performance of the NCG algorithm

on recovering the mKdV breathers situated on a zero background. The expression for the two-parameter family of zero-mean mKdV breathers in the envelope reference frame $u(x,t) = \beta(x - ct, t)$ is [58]

$$\beta(\chi, \tau; \kappa_1, \kappa_2) = 2\sqrt{2}\kappa_1 \text{sech}(\Theta) \frac{\cos(\Xi) - \frac{\kappa_1}{\kappa_2} \sin(\Xi) \tanh(\Theta)}{1 + \left(\frac{\kappa_1}{\kappa_2}\right)^2 \sin^2(\Xi) \text{sech}^2(\Theta)}, \quad (A2)$$

where, without loss of generality, the two solution parameters are positive $\kappa_{1,2} > 0$. These parameters are related to the velocity of the envelope $c = \kappa_1^2 - 3\kappa_2^2$ and the nonlinear angular frequency of carrier oscillations $\omega = -\Xi_t = -\kappa_2(\kappa_2^2 - 3\kappa_1^2)$ in the stationary reference frame [59]. Additionally, $\Xi(\chi, \tau)$ and $\Theta(\chi)$ are

$$\Xi(\chi, \tau) = \kappa_2 \left[\chi - 2(\kappa_2^2 + \kappa_1^2) \tau \right],$$

$$\Theta(\chi) = \kappa_1 \chi.$$
 (A3)

There are two distinguished limits of breather solutions to the mKdV equation: (a) the weakly nonlinear NLS regime $(\kappa_1/\kappa_2 \ll 1)$ and (b) the strongly nonlinear regime $[\kappa_1/\kappa_2 \sim O(1)]$ where breathers tend to double-pole solutions [60]. For $T=2\pi/\Omega=3.1105$, where Ω is the angular frequency of oscillations in the envelope reference frame, we recover both the distinguished limits using the Newton-conjugate gradient algorithm, coupled to a c-continuation line search. Our computational parameters are $\Delta x=0.05$, $\Delta t\approx 0.1$, and the computational spatial domain 2L=400. Along the entire constant T path on the c- Ω plane, the space-time infinity norm of the error in the numerical solution is kept approximately 10^{-7} . The results of numerical continuation are summarized in Fig. 12.

- [20] A. J. Whitfield and E. R. Johnson, Phys. Rev. E 91, 051201(R) (2015).
- [21] K. Nakayama and K. Lamb, J. Fluid Mech. 903, A40 (2020).
- [22] H. Leblond and D. Mihalache, Phys. Rep. 523, 61 (2013).
- [23] A. Hasegawa and Y. Kodama, *Solitons in Optical Communications*, Oxford Series in Optical and Imaging Sciences Vol. 7 (Oxford University Press, Oxford, 1995).
- [24] Y. S. Kivshar and B. Luther-Davies, Phys. Rep. **298**, 81 (1998).

^[1] M. J. Ablowitz and H. Segur, *Solitons and Inverse Scattering Transform* (SIAM, Philadelphia, 1981).

^[2] S. Clarke, R. Grimshaw, P. Miller, E. Pelinovsky, and T. Talipova, Chaos 10, 383 (2000).

^[3] M. Onorato, S. Residori, U. Bortolozzo, A. Montina, and F. Arecchi, Phys. Rep. 528, 47 (2013).

^[4] E. A. Kuznetsov and A. V. Mikhailov, Zh. Eksp. Teor. Fiz. 67, 1717 (1974) [Sov. Phys. JETP 40, 855 (1975)].

^[5] X.-R. Hu, S.-Y. Lou, and Y. Chen, Phys. Rev. E 85, 056607 (2012).

^[6] X.-P. Cheng, S. Y. Lou, C.-l. Chen, and X.-Y. Tang, Phys. Rev. E 89, 043202 (2014).

^[7] B. Ren and J. Lin, Z. Naturforsch. A 70, 539 (2015).

^[8] J. Chen and D. E. Pelinovsky, J Nonlinear Sci. 29, 2797 (2019).

^[9] D. E. Pelinovsky and R. E. White, Proc. R. Soc. A 476, 20200490 (2020).

^[10] M. Bertola, R. Jenkins, and A. Tovbis, Nonlinearity 36, 3622 (2023).

^[11] M. A. Hoefer, A. Mucalica, and D. E. Pelinovsky, J. Phys. A: Math. Theor. 56, 185701 (2023).

^[12] S. Flach and A. V. Gorbach, Phys. Rep. 467, 1 (2008).

^[13] G. James, Philos. Trans. R. Soc. A 376, 20170138 (2018).

^[14] D. K. Campbell, J. F. Schonfeld, and C. A. Wingate, Physica D 9, 1 (1983).

^[15] J. P. Boyd, Nonlinearity **3**, 177 (1990).

^[16] M. D. Maiden and M. A. Hoefer, Proc. R. Soc. A 472, 20160533 (2016).

^[17] Y. Mao, S. Chandramouli, W. Xu, and M. A. Hoefer, Phys. Rev. Lett. **131**, 147201 (2023).

^[18] K. G. Lamb, O. Polukhina, T. Talipova, E. Pelinovsky, W. Xiao, and A. Kurkin, Phys. Rev. E 75, 046306 (2007).

^[19] R. Grimshaw and K. Helfrich, Stud. Appl. Math. 121, 71 (2008).

- [25] D. Mandelik, H. S. Eisenberg, Y. Silberberg, R. Morandotti, and J. S. Aitchison, Phys. Rev. Lett. 90, 253902 (2003).
- [26] T. Schäfer and C. Wayne, Physica D 196, 90 (2004).
- [27] A. Sakovich and S. Sakovich, J. Phys. Soc. Jpn. 74, 239 (2005).
- [28] A. Di Carli, C. D. Colquhoun, G. Henderson, S. Flannigan, G.-L. Oppo, A. J. Daley, S. Kuhr, and E. Haller, Phys. Rev. Lett. 123, 123602 (2019).
- [29] D. Luo, Y. Jin, J. H. V. Nguyen, B. A. Malomed, O. V. Marchukov, V. A. Yurovsky, V. Dunjko, M. Olshanii, and R. G. Hulet, Phys. Rev. Lett. 125, 183902 (2020).
- [30] B. Kalinikos, N. Kovshikov, and A. Slavin, J. Appl. Phys. 67, 5633 (1990).
- [31] A. B. Ustinov, N. Y. Grigor'eva, and B. A. Kalinikos, JETP Lett. 88, 31 (2008).
- [32] A. Drozdovskii, M. Cherkasskii, A. B. Ustinov, N. Kovshikov, and B. A. Kalinikos, JETP Lett. 91, 16 (2010).
- [33] K. R. Helfrich, Phys. Fluids 19, 026601 (2007).
- [34] A. I. Dyachenko and V. E. Zakharov, JETP Lett. 88, 307 (2008).
- [35] A. E. Kudryavtsev, JETP Lett. 22, 82 (1975).
- [36] M. J. Ablowitz, M. D. Kruskal, and J. F. Ladik, SIAM J. Appl. Math. 36, 428 (1979).
- [37] H. Segur and M. D. Kruskal, Phys. Rev. Lett. 58, 747 (1987).
- [38] A. Soffer and M. I. Weinstein, Invent. Math. 136, 9 (1999).
- [39] H. Kalisch, M. A. Alejo, A. J. Corcho, and D. Pilod, arXiv:2201.12074.
- [40] A. V. Mikhailov, V. S. Novikov, and J. P. Wang, Stud. Appl. Math. 118, 419 (2007).
- [41] N. Costanzino, V. Manukian, and C. K. Jones, SIAM J. Math. Anal. 41, 2088 (2009).
- [42] J. Yang, J. Comput. Phys. 228, 7007 (2009).

- [43] J. Yang, Stud. Appl. Math. 134, 420 (2015).
- [44] D. H. Peregrine, J. Fluid Mech. 25, 321 (1966).
- [45] T. B. Benjamin, J. L. Bona, and J. J. Mahony, Philos. Trans. R. Soc. London Ser. A **272**, 47 (1972).
- [46] P. J. Olver, Math. Proc. Cambridge 85, 143 (1979).
- [47] P. Olson and U. Christensen, J. Geophys. Res. 91, 6367 (1986).
- [48] N. K. Lowman and M. A. Hoefer, Phys. Rev. E 88, 023016 (2013).
- [49] S. Harris, Nonlinearity 9, 187 (1996).
- [50] M. A. Johnson and W. R. Perkins, SIAM J. Math. Anal. 52, 277 (2020).
- [51] M. J. Ablowitz, Nonlinear Dispersive Waves: Asymptotic Analysis and Solitons (Cambridge University Press, Cambridge, 2011), Vol. 47.
- [52] G. B. Whitham, *Linear and Nonlinear Waves* (Wiley, New York, 2011).
- [53] C. Ward, P. Kevrekidis, and N. Whitaker, Phys. Lett. A 383, 2584 (2019).
- [54] C. B. Ward, P. G. Kevrekidis, T. P. Horikis, and D. J. Frantzeskakis, Phys. Rev. Res. 2, 013351 (2020).
- [55] Y. S. Kivshar and V. V. Afanasjev, Phys. Rev. A 44, R1446 (1991).
- [56] T. Congy, G. A. El, M. A. Hoefer, and M. Shearer, Stud. Appl. Math. 147, 1089 (2021).
- [57] J. Yang, Nonlinear Waves in Integrable and Nonintegrable Systems (SIAM, Philadelphia, 2010).
- [58] M. Wadati, J. Phys. Soc. Jpn. 34, 1289 (1973).
- [59] G. L. Lamb, Jr., Elements of Soliton Theory (Wiley, New York, 1980), p. 29.
- [60] M. Wadati and K. Ohkuma, J. Phys. Soc. Jpn. 51, 2029 (1982).